

Spectral Image Tokenizer

Carlos Esteves

Mohammed Suhail

Ameesh Makadia

{machc, suhailmhd, makadia}@google.com

Google Research

Abstract

Image tokenizers map images to sequences of discrete tokens, and are a crucial component of autoregressive transformer-based image generation. The tokens are typically associated with spatial locations in the input image, arranged in raster scan order, which is not ideal for autoregressive modeling. In this paper, we propose to tokenize the image spectrum instead, obtained from a discrete wavelet transform (DWT), such that the sequence of tokens represents the image in a coarse-to-fine fashion. Our tokenizer brings several advantages: 1) it leverages that natural images are more compressible at high frequencies, 2) it can take and reconstruct images of different resolutions without retraining, 3) it improves the conditioning for next-token prediction – instead of conditioning on a partial line-by-line reconstruction of the image, it takes a coarse reconstruction of the full image, 4) it enables partial decoding where the first few generated tokens can reconstruct a coarse version of the image, 5) it enables autoregressive models to be used for image upsampling. We evaluate the tokenizer reconstruction metrics as well as multiscale image generation, text-guided image upsampling and editing.

1. Introduction

In natural language processing (NLP), tokenization associates words or parts of words to entries in a fixed vocabulary, which is straightforward since language is inherently discrete. The sequence of discrete tokens is suitably modeled as a categorical distribution with autoregressive (AR) transformers, which is the foundation of modern large language models (LLMs) [28, 36, 37].

While natural images are represented by discrete pixel values, they exhibit high dimensionality, redundancies, and noise that make it impractical to associate one token per pixel. This motivated a long line of research of learnable image tokenizers [14, 29, 29, 41, 44]. While there are

successful autoregressive image generation models [14, 44, 45], images are not sequential like language, which motivated developing alternatives to AR models such as denoising diffusion models [11, 30, 34] and masked transformers [3, 4]. Nevertheless, most of these alternatives also operate on the latent space of tokenizers like VQGAN [14] instead of raw pixels.

In this work, we revisit AR transformer-based image generation. Our main contribution is a tokenizer operating on the image spectrum, where the coarse-to-fine representation lends itself more naturally to a sequential interpretation.

Our Spectral Image Tokenizer (SIT) has several useful properties and enables different applications:

1. Since the power spectrum of natural images decreases with frequency, high frequencies can be more heavily compressed with little effect in visual quality. SIT leverages this by associating tokens to larger patches at higher wavelet scales than at lower scales (see Fig. 2).
2. SIT is transformer-based [42]; by using an attention mask where each scale depends on itself and lower scales (dubbed “Scale-Causal attention”), SIT can be trained at a single resolution and used to tokenize images of multiple resolutions (any number of scales up to the trained maximum), and detokenize partial token sequences (up to some scale), reconstructing a coarse image.
3. Using SIT, we train an autoregressive generative transformer (AR-SIT) that models images coarse-to-fine. The next-token prediction is then conditioned on a coarse reconstruction of the image given by the partial token sequence, instead of the usual conditioning on the partial reconstruction of the previous rows of the image.
4. AR-SIT can quickly decode only the first few tokens and reconstruct a coarse version of the image, enabling applications like quickly showing multiple coarse generations and letting the user select which ones to refine.
5. AR-SIT can be used for text-based upsampling of an input low resolution image, by starting the decoding process with the few tokens output by SIT, and generating the rest of the sequence up to a desired resolution.

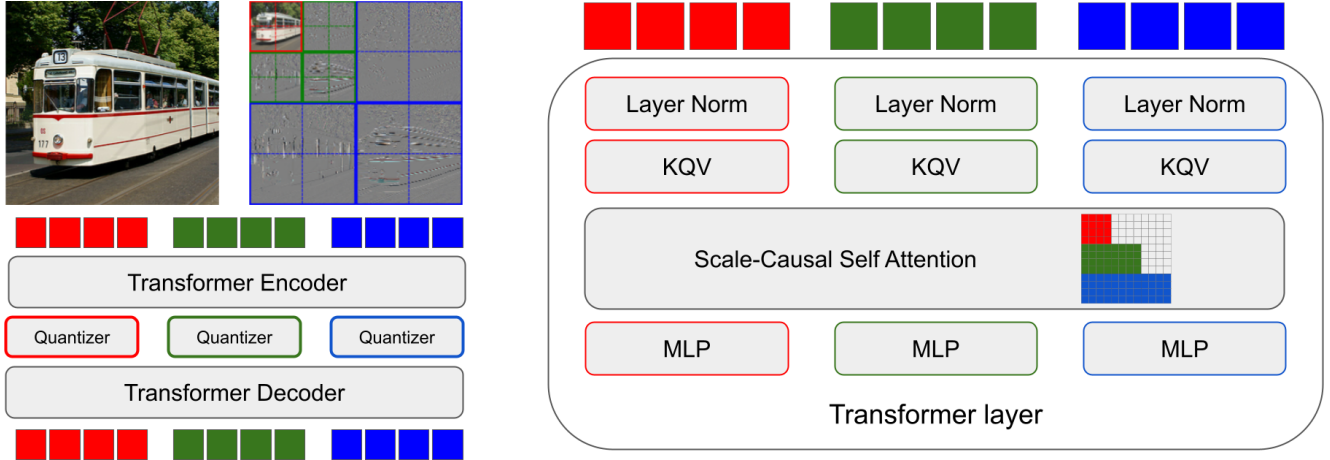


Figure 1. *Left*: we introduce a Spectral Image Tokenizer (SIT), that learns to encode and decode discrete wavelet transform (DWT) coefficients to and from a small set of discrete tokens, such that the sequence represents the image in a coarse-fine fashion. SIT is naturally multiscale and enables coarse-to-fine autoregressive image generation with our AR-SIT model. SIT also leverages the sparsity of high frequency coefficients in natural images. *Right*: details of the encoder/decoder transformer layers. The main architectural difference with respect to previous tokenizers is that the distribution of each DWT scale is distinct, hence we use specialized parameters for each scale, such as the quantizer codebooks and inner transformer layers. We also introduce a scale-causal attention where each token attends to its own scale and lower scales, which enables encoding, decoding, generating, and upsampling images at different resolutions.

- AR-SIT can be used for text-guided image editing, by encoding a given image only up to a coarse scale, and generating the finer details conditioned on a new caption.

Currently, image generation is dominated by diffusion models such as Imagen 3 [18], DALL-E-3 [1] and Stable Diffusion 3 [15]. On the other hand, large language models (LLMs) such as Gemini [36], GPT-4 [28], and Llama 3 [37] are based on autoregressive transformers. We believe autoregressive image generation is still worth pursuing because it might benefit from advances in LLMs, and multimodal applications might benefit of having a single architecture for all modalities. Recent work on image and video generation support this point [35, 38, 46]. Dieleman [12] recently interpreted denoising diffusion models as spectral autoregression, since, when looking at image spectra, the denoising procedure uncovers frequencies from low to high. In contrast, our method does literal spectral autoregression.

2. Related work

Image tokenization Several methods have been developed to map images to a small set of discrete tokens suitable for generative modeling. VQ-VAE [41] introduced vector-quantization in the latent space of a Variational Auto-Encoder to map images, audio and video to a set of discrete values. VQGAN [14] improved upon VQVAE by using perceptual and adversarial losses. We build on ViT-VQGAN [44], which improved upon VQGAN by using a Vision Transformer (ViT) [13] instead of convolutions, as well as codebook factorization and feature normalization.

In this paper, we are interested in multiscale image representations. VQ-VAE-2 [29] introduced multiscale latents by keeping and quantizing intermediate downsampled convolutional features. RQ-VAE [21] quantized a set of residuals such that the latent vector is represented in a coarse-to-fine fashion and reconstructed by adding the code embeddings for each residual. Similarly, VAR [38] and STAR [23] split the latent space in multi-scale quantized residuals, so that it can be reconstructed by upsampling and summing. The crucial difference between our approach and the aforementioned is that we operate on spectral coefficients of the input and not on latent features. This allows our tokenizer to be truly multiscale so that it can take inputs at different scales and reconstruct up to some scale, while also leveraging that higher frequencies are more compressible in natural images.

Tangentially related to our work, Wave-ViT [43] modified the ViT self-attention by applying a DWT to the input and concatenating coefficients, effectively exchanging space for depth to reduce the sequence length. Zhu and Soricut [48] modified the ViT patchifier in a similar way, and introduced patch embeddings that leverage the sparsity of high frequency coefficients. Both methods are for discriminative tasks such as image classification and segmentation, while we focus on generation.

Autoregressive image generation Early approaches PixelRNN and PixelCNN [39, 40] generate images pixel by pixel by modeling the conditional distribution of the pixel given the previous pixels with recurrent layers of causal convolutions. PixelSNAIL [5] improved on this model by introducing self-attention layer to better model long-range

dependencies. VQ-VAE [41] introduced a two-stage approach with a tokenizer and a separate stage to model the distribution of tokens. VQGAN [14] greatly improved these results by both improving the tokenizer and using a transformer to model the distribution. Finally, ViT-VQGAN [44] proposed a transformer-based tokenizer, which Parti [45] used with a large autoregressive transformer capable of high-quality text-to-image generation.

MaskGIT [3] and Muse [4] highlighted the disadvantages of the typical autoregressive models raster-order conditioning, and proposed to generate all tokens in parallel iteratively, where each iteration keeps the highest confidence tokens. We address the same problem with a tokenizer whose sequence represents the image in a coarse-to-fine order instead of raster-order.

Multiscale image generation Multiscale image generation ideas have appeared in the context of VAEs [2], GANs [19, 31], and diffusion models [16, 20, 32], but have not been sufficiently explored with AR transformers.

Nash et al. [27] represented an image as a sequence of quantized and thresholded DCT coefficients, where the compression comes from the fact that many coefficients are zero and are omitted. By sorting the sequence by frequency, the method can model images from coarse-to-fine like we do. However, the compressed representation is handcrafted and results in long sequences. In a similar vein, Mattar et al. [25] handcrafted a tokenizer based on DWT coefficients, introducing tokens to represent large chunks of zeros. It also results in long sequences and is only applied to generations of small grayscale images. In contrast with these methods, instead of handcrafting a compressed input representation, our tokenizer learns to encode to, and decode from, a short compressed coarse-to-fine sequence.

3. Background

A discrete wavelet transform (DWT) is based on successive convolutions of the signal f with a pair of lowpass g and highpass h filters with the first step as follows

$$f_{\text{low}_1}[n] = f \star g = \sum_k f[k]g[n-k], \quad (1)$$

$$f_{\text{high}_1}[n] = f \star h = \sum_k f[k]h[n-k]. \quad (2)$$

The high and low outputs are subsampled by a factor of two, and the operation is repeated for the low channel, such that at level L we compute $f_{\text{low}_L} = f_{\text{low}_{L-1}} \star g$ and $f_{\text{high}_L} = f_{\text{low}_{L-1}} \star h$, subsample again and drop $f_{\text{low}_{L-1}}$. The output at level L comprises the approximation coefficients f_{low_L} and the detail coefficients $\{f_{\text{high}_k}\}$ for $1 \leq k \leq L$. This output has the same cardinality as the input and the transformation is invertible, where the forward transform is typically called “analysis” and the backward “synthesis”.

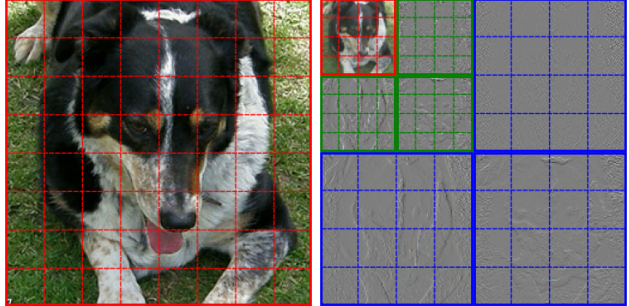


Figure 2. Input patchification. *Left*: typical patchification for Vision Transformers (ViT) [13], where the image is split in equal-sized patches. *Right*: we propose to patchify the coefficients of a discrete wavelet transform (DWT) instead. Each scale is shown in a different color. Scales other than the lowest contain three blocks representing horizontal, vertical and diagonal details; we concatenate the spatially correspondent patches of each block such that each scale is represented by the same sequence length. This results in larger patch sizes for higher scales, which are more compressible. The figure shows 3 scales and 16 tokens per scale; in our experiments we use 4 or 5 scales and 256 tokens per scale.

The simplest wavelet family is the Haar, where $g = [1, 1]^\top$ and $h = [1, -1]^\top$ (optionally scaled to unit norm).

For image analysis we use a 2D DWT, which is obtained by simply convolving the rows and columns with g and h . The approximation coefficients $f_{\text{low}_1} = f \star (gg^\top)$, and the details are divided into horizontal $f_{\text{H}_1} = f \star (gh^\top)$, vertical $f_{\text{V}_1} = f \star (hg^\top)$ and diagonal $f_{\text{D}_1} = f \star (hh^\top)$ details. Subsequent levels apply the same operations to the approximation coefficients. Fig. 2 shows a two-level transform, where we can see that the approximation coefficients correspond to a coarse version of the image.

We refer to the textbooks by Mallat [24] and Daubechies [9] for more information about wavelets.

4. Method

Our main contribution, SIT, is an image tokenizer that takes discrete wavelet transform (DWT) coefficients. The model follows ViT-VQGAN [44], with important changes that we describe in this section and visualize in Fig. 1. For image generation, we introduce AR-SIT which is based on Parti [45] with minor changes, using SIT as the tokenizer.

4.1. Tokenizer

Patchification and featurization The first step is to map the input to a sequence of patches. We apply the Haar DWT on the input image and patchify each scale separately. While Haar is the simplest wavelet and lacks properties found in other wavelets useful for compression, we found no benefits of using other wavelet families such as CDF [8].

Our design choice is to use the same number of patches

for each scale. In a DWT, the higher scales correspond to high frequency details which are represented by more coefficients than the lower scales, but contribute less to the spatial pixel values. In other words, in natural images, most of the power spectrum is concentrated on lower frequencies. By representing each scale with the same number of tokens, we are compressing more the higher frequencies (since they are represented by more coefficients), similarly to what is done in image compression methods such as JPEG2000 [7].

The approximation (or lowpass) DWT coefficients correspond to a coarse version of the input image, which we consider the first scale. The following scales are divided in three blocks corresponding to horizontal, vertical, and diagonal details, where each coefficient relates to a specific spatial location. Thus, we can concatenate the three blocks such that each entry corresponds to the same spatial location. For example, the first scale will typically be split in patches that are $32 \times 32 \times 3$, with channels corresponding to RGB, the second scale will be $32 \times 32 \times 9$, where the channels correspond to the RGB of horizontal, vertical, and diagonal details, the third will be $64 \times 64 \times 9$ and so on. Fig. 2 shows an example of our patchification scheme.

Since patches have different resolutions (higher scales will have larger patches), the usual ViT linear embedding to map patches to features cannot be shared across all patches so we have different parameters per scale. Formally, given an image f , our patchifiers compute

$$f_{\text{low}_L}, \{f_{H_i}\}_{i \leq L}, \{f_{V_i}\}_{i \leq L}, \{f_{D_i}\}_{i \leq L} = \text{DWT}(f), \quad (3)$$

$$c_1 = P_0(f_{\text{low}_L}), \quad (4)$$

$$c_s = P_s(f_{H_{L-s+2}}, f_{V_{L-s+2}}, f_{D_{L-s+2}}), \quad 1 < s \leq L, \quad (5)$$

where $c_s = \{c_s^n\}_{1 \leq n \leq N}$ is the sequence of token embeddings at scale s , and $c_s^n \in \mathbb{R}^C$ is the embedding of the n -th token at the s -th scale, while L is the number of DWT levels, $S = L + 1$ is the number of scales and N the number of tokens per scale. For brevity, when there is no ambiguity, we may omit the set indexing and use $\{c_s\}$ to denote the set of tokens of all scales, for example.

The final projection after the decoder needs to map the features back to different sized patches, so it also has different parameters per scale. Those patches still represent DWT coefficients so an inverse DWT (IDWT) is finally applied to obtain an image output.

Flexible sequence length The tokenizer encoder and decoder transformers operate on the sequence of patch features of length SN . The sequence length is a major factor in resource utilization so we want to keep it constrained. Our method is flexible since we can choose the number of scales and the patch size per scale, while most ViT-based models such as ViT-VQGAN [44] are more restricted. They use the same patch size for the whole image; thus, keeping the same patch size and doubling each image dimension would

increase the sequence length by a factor of 4, where our method is capable of including additional scales which only increases the sequence length by multiples of N .

For example, for a 256×256 input, the ViT-VQGAN baseline uses 8×8 patches to obtain a sequence of 1024 elements. Our method can use 4 scales and 256 tokens per scale for the same sequence length. When increasing the resolution to 512×512 , the baseline can either increase the patch size to 16×16 , resulting in the same sequence length, or keep it 8×8 , resulting in a $4 \times$ longer sequence. Our method, for example, can vary the number of scales from 4 to 6, resulting in sequence lengths of 1024, 1280, 1536 which are more manageable. Sec. 5.2 shows results with high-resolution reconstruction.

Transformers After featurization, the single sequence containing all scales passes through a transformer encoder, followed by quantization and a transformer decoder. We propose two optional modifications to the transformers, which are otherwise identical to the ones used in ViT [13].

First, we propose a scale-causal attention mask, where an element at some scale attends to all elements of its own scale and lower scales, represented by a block-triangular mask pattern. With dense attention, we write the application of the encoding transformer T_{enc} as $\{z_s\} = T_{\text{enc}}(\{c_s\})$, and for scale-causal we write $z_s = T_{\text{enc}}(\{c_k\}_{1 \leq k \leq s})$ for each s . The scale-causal attention can be applied independently to the encoder and decoder, enabling different applications. For the multiscale reconstruction experiments in Sec. 5.1, we need to both encode and decode multiple resolutions, so both encoder and decoder use scale-causal masks. For coarse-to-fine image generation in Sec. 5.3, only the decoder needs to be scale-causal in order to decode the partially generated sequence. For the text-guided image upsampling in Sec. 5.4, only the encoder needs to be scale-causal to encode the lower resolution inputs. For the image editing experiments in Sec. 5.5, the scale-causal encoder prevents information leaking from high to low scale.

Second, we propose to use different transformer parameters per scale. In our model, the subsequences corresponding to coefficients of each scale come from quite distinct distributions, so it makes sense to treat them differently. This contrasts with the case of natural images where each patch can be considered as coming from the same distribution. Thus, the parameters of the key, query, and value embeddings, the layer norms, and the MLP on each transformer layer are shared per scale but not across scales. The transformer still takes a single sequence composed of all scales; we experimented with different transformers per sequence with cross-attention for information sharing, but it performed worse. Note that this change leads to significantly more memory utilization to store the extra parameters, but the training/inference speed is similar because the number of operations is unchanged.

Table 1. Multiscale reconstruction on ImageNet. ‘‘SC’’ denotes scale-causal attention, which slightly reduces performance at the highest resolution but enables multiscale reconstruction without downsampling/upsampling or retraining. The ViT-VQGAN values from Yu et al. [44] used a logit-laplace loss which was later considered harmful [45], so we retrain without it. Our SIT improves reconstruction metrics and is significantly faster at lower resolutions. We report test time throughput of an encoding/decoding cycle for the max batch size that fits on a TPU v5e.

	LPIPS ↓	PSNR ↑	L1 ↓	FID ↓	IS ↑	images/s ↑
<i>Resolution: 256 × 256</i>						
ViT-VQGAN (reported)	-	25.1	0.031	1.55	190.2	-
ViT-VQGAN	0.144	24.5	0.036	1.07	197.3	159
SIT (ours)	0.138	25.2	0.033	1.33	196.7	-
SIT-SC (ours)	0.152	25.0	0.035	1.56	193.3	132
<i>Resolution: 128 × 128</i>						
ViT-VQGAN	0.161	26.8	0.029	3.01	121.1	159
SIT-SC (ours)	0.159	27.3	0.027	2.18	130.8	159
<i>Resolution: 64 × 64</i>						
ViT-VQGAN	0.117	30.0	0.021	3.30	22.5	159
SIT-SC (ours)	0.123	30.2	0.020	1.63	30.4	215
<i>Resolution: 32 × 32</i>						
ViT-VQGAN	0.089	28.8	0.024	5.27	3.6	159
SIT-SC (ours)	0.048	33.6	0.014	0.65	3.6	253
<i>Resolution: 16 × 16</i>						
ViT-VQGAN	0.044	30.2	0.021	1.75	1.8	159
SIT-SC (ours)	0.035	35.4	0.011	0.41	1.8	850

Quantizer The encoder outputs a sequence of features that are quantized to a fixed-sized codebook, similarly to ViT-VQGAN [44] and prior works VQVAE [41], VQGAN [14]. We modify the quantizer such that each scale has a different codebook for the same reasons discussed in the previous paragraph. Thus, each codebook size and feature dimension are the same as the ViT-VQGAN baseline, but we have different features for the same code at different scales. Formally, we apply $q_s^n = Q_s(z_s^n)$ for each pair (s, n) , where q_s^n is chosen from the codebook for s and thus can be associated with its discrete position in the codebook, denoted $\lfloor q_s^n \rfloor$. We found that including an entropy loss similar to MaskGIT [3] and MAGVIT-v2 [46] improves reconstruction quality. Let d_{snj} be the softmax-normalized similarities between the pre-quantized features z_s^n and the j -th entry of the s -th codebook. To encourage sharp association between each feature and its assigned code, we add loss terms to minimize the entropies $H_{sn} = -\sum_j d_{snj} \log d_{snj}$. To encourage that all codebook entries are similarly utilized, we compute $p_{sj} = 1/N \sum_n d_{snj}$ and maximize the entropies $H_s = -\sum_j p_{sj} \log p_{sj}$.

Training We follow the ViT-VQGAN training protocol and use the same weighting for the L2, perceptual, adversarial, and quantization losses. We remove the logit-laplace loss that was shown detrimental in follow-up work [45], and we add the entropy loss mentioned before.

Table 2. Coarse-to-fine image generation, evaluated on MSCOCO [22]. With SIT, the autoregressive generation is stopped early for a coarse version of the image. The Parti350M baseline does not have this property, so we generate at full resolution and downsample for comparison. AR-SIT is several times faster and more memory efficient than the baselines at lower resolutions, with little loss of quality, even when trained only on higher resolution data. We report throughput and memory utilization during generation given the max batch size that fits on a TPU v5e.

	FID ↓	IS ↑	images/s ↑	Gb/image ↓
<i>Resolution: 256 × 256</i>				
Parti350M (reported)	14.1	-	-	-
Parti350M	12.3	36.5	2.5	2.0
AR-SIT-SCD-4 (Ours)	13.7	34.3	2.5	2.0
<i>Resolution: 128 × 128</i>				
Parti350M	10.8	33.9	2.5	2.0
AR-SIT-SCD-4 (Ours)	11.5	31.7	4.8	1.0
<i>Resolution: 64 × 64</i>				
Parti350M	10.7	18.1	2.5	2.0
AR-SIT-SCD-4 (Ours)	11.3	17.7	10.1	0.7
<i>Resolution: 32 × 32</i>				
Parti350M	6.5	3.0	2.5	2.0
AR-SIT-SCD-4 (Ours)	7.0	3.1	54.5	0.3

All losses are applied to the spatial domain images reconstructed by the inverse discrete wavelet transform on the decoder output: $\hat{f} = \text{IDWT}(T_{\text{dec}}(\{q_s\}))$. We noticed instability during training due to the adversarial loss, which was fixed by applying spectral normalization following Miyato et al. [26], which simply divides the discriminator weight matrices by their largest singular value.

4.2. Autoregressive image generation

We use our tokenizer for autoregressive image generation, by training a second stage transformer model similar to Parti [45], with some modifications. Formally, the autoregressive transformer T models categorical distributions over the discrete codes

$$P(\lfloor q_s^n \rfloor) = T(\{\lfloor q_i \rfloor\}_{1 \leq i < s} \cup \{\lfloor q_s^i \rfloor\}_{1 \leq i < n}), \quad (6)$$

which can be sampled one code at a time for generation. T can be conditioned on a textual description processed by a transformer encoder for text-to-image generation. For training, we model the distribution of input codes as $P(\{\lfloor q_s \rfloor\}) = \prod_{1 \leq s \leq S} P(\lfloor q_s^n \rfloor)$ and minimize the negative log-likelihood $-\log P(\{\lfloor q_s \rfloor\})$ over the training set.

Since we use different codebooks per scale, the same discrete token id appearing at different scales has different meanings. Thus, we use different token embeddings per

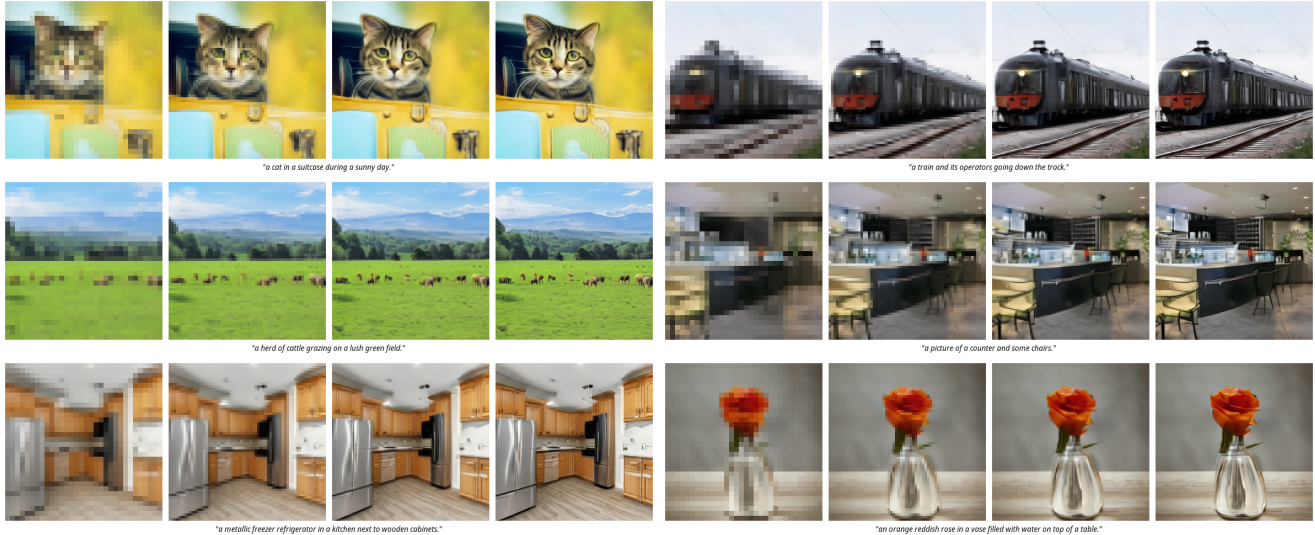


Figure 3. Coarse-to-fine text-to-image on MS-COCO [22] prompts. Each quadruple shows generations from AR-SIT-SCD for the given prompt, where, from left to right, only the first 25%, 50%, 75% and 100% of tokens are generated, corresponding to resolutions of 32×32 to 256×256 , where only 256×256 images are seen during training. Our model enables quick generation of coarse image candidates that can be further improved if needed.

scale in the second stage. For similar reasons, the last layer for logit prediction is also different for each scale.

For the generative applications described in Secs. 5.3 and 5.4, we introduce mild changes in order to interrupt the generation after all tokens up to a certain scale are generated, and to start the generation with given tokens up to a certain scale.

5. Experiments

5.1. Multiscale reconstruction

In this experiment, we train our tokenizer on ImageNet [10] and evaluate its reconstruction performance. We follow the ViT-VQGAN [44] “Base” architecture (12 layers and 768/3072 channels) and training protocol.

The model denoted “SIT” is the Spectral Image Tokenizer with 5 scales from 16×16 to 128×128 resolutions, where each scale is represented by 256 tokens. The variation “SIT-SC” uses scale-causal attention on both the encoder and decoder, which enables handling inputs and outputs of different resolutions, even though it is only trained at 256×256 . For example, when the input image is 64×64 , only the first two scales are used, resulting in shorter sequence lengths which reduces memory utilization and processing time. Both models employ the variant described in Sec. 4.1 that use different transformer parameters per scale.

The ViT-VQGAN baseline only works for 256×256 inputs, so to evaluate against it fairly, we upsampled the low-resolution inputs to that resolution. This brings the input patches away from the training distribution, which might

explain the drop in reconstruction quality.

Tab. 1 shows the reconstruction metrics while Fig. 6 shows reconstruction samples at multiple resolutions.

5.2. High-resolution reconstruction

Our main results are on 256×256 images, which is typical for autoregressive and masked transformers generative models [3, 4, 45], where separate superresolution stages are trained to enable higher resolution outputs.

Here we evaluate whether our multiscale tokenizer can scale to high resolution inputs. We rerun the multiscale reconstruction experiment in Sec. 5.1 for 512×512 inputs. We experiment SITs with 4 to 6 scales and 256 tokens per scale. For the baseline we increase the patch size from 8×8 to 16×16 . If we were to keep the same patch size for the baseline, the sequence length would increase by a factor of 4 to 4096, which is too costly.

Interestingly, the ViT-VQGAN baseline suffered with heavy instability during training, which was not resolved by reducing the learning rate, using spectral normalization, or the logit-laplace loss. In contrast, all SIT variations trained successfully with no hyperparameter changes.

Tab. 3 shows the results, which suggest that the SITs scale better than spatial tokenizers to higher resolutions, and might enable autoregressive generation of high resolution images without a separate superresolution model.

5.3. Coarse-to-fine text-to-image generation

We tackle text-to-image generation by using an autoregressive transformer to model the distribution of discrete tokens

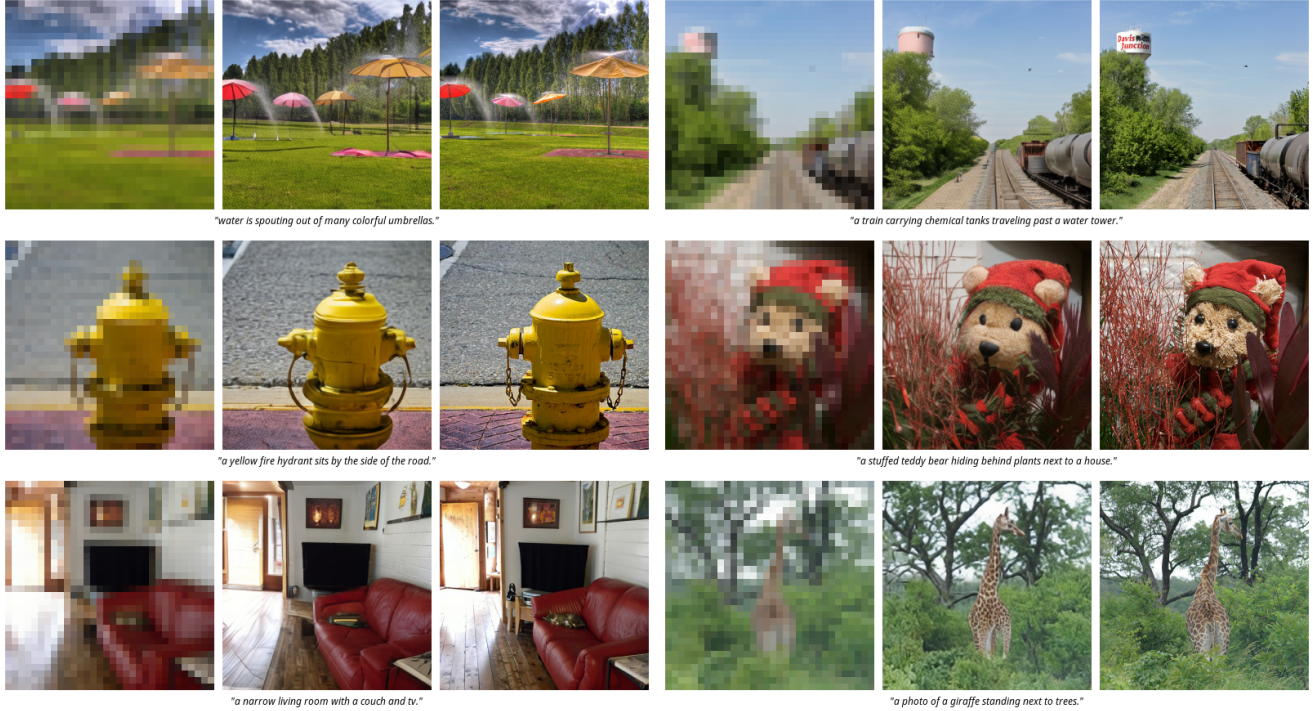


Figure 4. Text-guided image upsampling on MS-COCO [22]. Our coarse-to-fine generative models can take a low-resolution image, encode it as the first few tokens of a sequence, and generate the rest of sequence, which, when decoded, effectively upsamples the input. Each triplet shows the given 32×32 image, our 256×256 reconstruction and the ground truth.

Table 3. Multiscale reconstruction on ImageNet at 512×512 resolution. We evaluate our SIT models for different number of scales denoted as the suffix, and the reconstruction quality improves with more scales. The ViT-VQGAN baseline suffered from heavy instability during training so we selected the best values before divergence. Results suggest that spectral tokenizers scale better to high resolutions than the spatial baselines.

	LPIPS ↓	PSNR ↑	FID ↓	IS ↑
VIT-VQGAN	0.320	22.44	6.92	151.5
SIT-4	0.262	22.92	3.51	177.5
SIT-5	0.248	23.60	2.67	188.8
SIT-6	0.245	23.52	2.95	188.4

output by our tokenizer. Since the SIT sequence of tokens represents an image in a coarse-fine fashion, the autoregressive model generation has the same property, which means that we can interrupt the generation after a certain number of tokens and decode a coarse version of the generation.

For this to work, the SIT decoder must be scale-causal, while there is no constraint for the encoder so we use dense attention (we denote this variant Scale-Causal Decoder, or “SIT-SCD”). It uses a “small” encoder and “large” decoder

as described in ViT-VQGAN [44], and 4 scales. To conserve memory, we share the transformer parameters for all scales in the decoder, while the encoder has different parameters per scale as described in Sec. 4.1.

We mostly follow the Parti350M [45] architecture and training protocol and name our generative model autoregressive SIT, or “AR-SIT”. Both SIT and AR-SIT are trained on a subset of WebLI [6] of around 128M images; given our batch sizes and number of training steps, each image is seen at most once during training. Evaluation is performed on 30k examples of MS-COCO [22]. We show metrics and generations at different resolutions in Fig. 3 and Tab. 2. While the metrics are slightly worse, the gap closes at lower resolutions and our generation is faster.

5.4. Text-guided image upsampling

We leverage the coarse-to-fine nature of SIT and apply a pre-trained text-to-image AR-SIT model for the task of text-guided image upsampling. Here we assume we are given a low resolution image and a caption.

The idea is to encode the low-resolution image, which will give the first tokens of our high resolution output. AR-SIT then takes these tokens and generates the rest of the sequence. For this to work, the SIT encoder must be scale-causal to properly tokenize low-resolution inputs, while

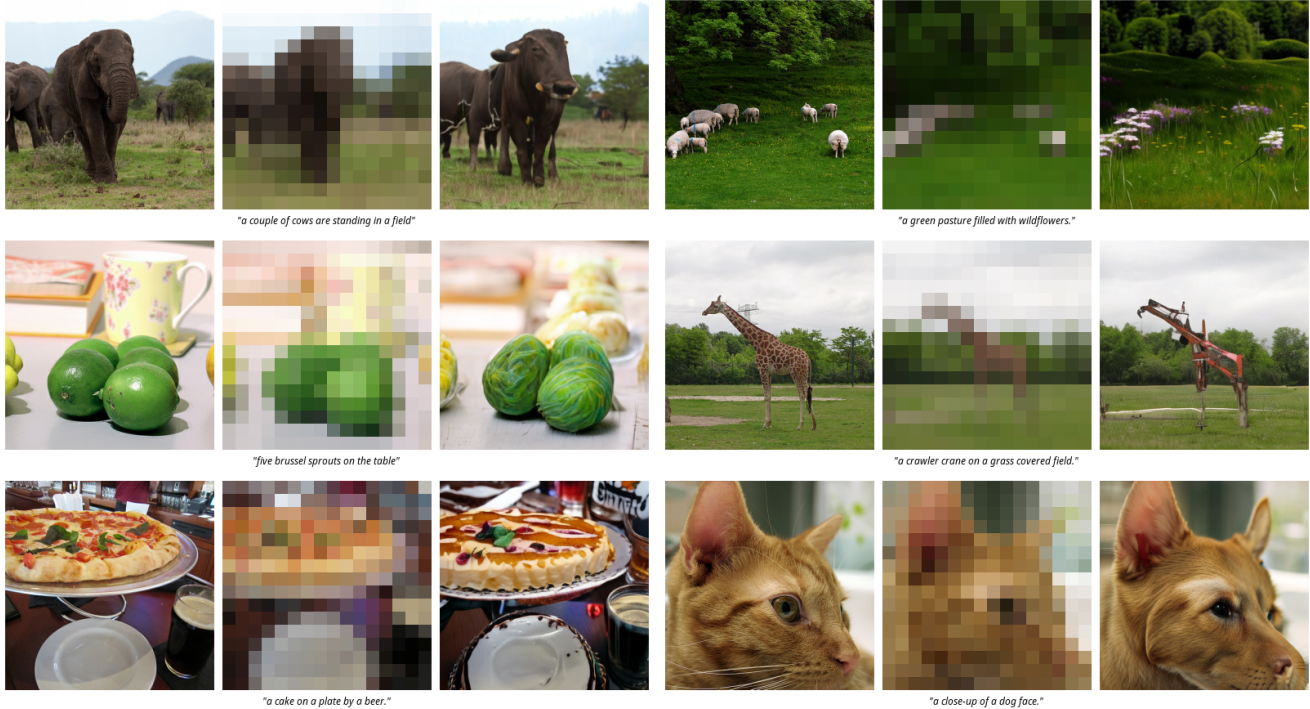


Figure 5. Text-guided image editing on MS-COCO [22]. Our coarse-to-fine generative models can do text-guided editing by encoding a given image but keeping only the lower scales, and using a pre-trained AR-SIT to re-generate the higher scales conditioned on the textual prompt. Each triplet shows the given image, its reconstruction using only the coefficients used to start the generation, and the edited image after generating the whole sequence.

there is no constraint for the decoder so we use dense attention. We denote this variant Scale-Causal Encoder, or “SIT-SCE”. The model is otherwise as the one used in Sec. 5.3.

In this experiment, the inputs are set to 32×32 . Fig. 4 shows some text-guided upsampling examples on MS-COCO [22]. We obtain an FID of 6.2 when evaluating the generations over the whole dataset, compared to 13.7 when given only the prompts. The appendix shows additional results upsampling from 16×16 inputs in Fig. 7, and metrics in Tab. 4.

5.5. Text-guided image editing

Our coarse-to-fine AR-SIT enables a text-guided image editing application, where we want to change image details while keeping the same overall appearance, which corresponds to freezing lower scales while generating higher.

We apply an AR-SIT trained only on the maximum likelihood objective as follows. The given image is tokenized only up to the first scale, corresponding to a coarse representation. The tokenizer encoder must be scale-causal in order to avoid leakage from high to low scales, so we use SIT-SCE here. Now we use AR-SIT to generate the rest of the sequence, conditioning on the textual caption.

In this experiment, we use a 5-scale model such that the

lowest resolution is 16×16 ; we found that starting with higher resolutions limits the changes the model can generate. Fig. 5 shows some examples of text-guided editing on MS-COCO [22], where we lightly modify the original captions, for example by swapping “elephants” with “cows”. We show additional results in Fig. 8 in the appendix.

6. Conclusion and limitations

We presented a spectral image tokenizer (SIT), and an autoregressive generative transformer trained with it (AR-SIT). SIT is naturally multiscale and leverages spectral properties of natural images for improved reconstruction quality. AR-SIT enables applications such as rapid generation of coarse images that can be refined later, and text-guided image upsampling and editing.

While our results show improvements on the tokenizer reconstruction accuracy, the AR generation still underperforms the baseline at the highest resolution. Chang et al. [4] similarly observed that a better tokenizer does not necessarily lead to a better generative model. Nevertheless, our method has multiscale properties and enables new applications not possible with prior work. We only experiment with a small AR-SIT of 350M parameters, while the Parti [45] baseline goes up to 22B parameters.

The supplementary material shows an ablation study, implementation details and additional results.

7. Acknowledgments

We thank Leonardo Zepeda-Núñez for reviewing this manuscript and offering interesting discussions and suggestions, and Jon Barron for sharing useful code we relied on.

References

- [1] James Betker, Gabriel Goh, Li Jing, † TimBrooks, Jianfeng Wang, Linjie Li, † LongOuyang, † JuntangZhuang, † JoyceLee, † YufeiGuo, † WesamManassra, † PrafullaDhariwal, † CaseyChu, † YunxinJiao, and Aditya Ramesh. Improving image generation with better captions. [2](#)
- [2] Lei Cai, Hongyang Gao, and Shuiwang Ji. *Multi-Stage Variational Auto-Encoders for Coarse-to-Fine Image Generation*, page 630–638. Society for Industrial and Applied Mathematics, 2019. [3](#)
- [3] Huiwen Chang, Han Zhang, Lu Jiang, Ce Liu, and William T. Freeman. Maskgit: Masked generative image transformer. In *CVPR*, 2022. [1, 3, 5, 6](#)
- [4] Huiwen Chang, Han Zhang, Jarred Barber, Aaron Maschinot, Jose Lezama, Lu Jiang, Ming-Hsuan Yang, Kevin Patrick Murphy, William T. Freeman, Michael Rubinstein, Yuanzhen Li, and Dilip Krishnan. Muse: Text-to-image generation via masked generative transformers. In *ICML*, 2023. [1, 3, 6, 8](#)
- [5] XI Chen, Nikhil Mishra, Mostafa Rohaninejad, and Pieter Abbeel. PixelSNAIL: An improved autoregressive generative model. In *ICML*, 2018. [2](#)
- [6] Xi Chen, Xiao Wang, Soravit Changpinyo, AJ Piergiovanni, Piotr Padlewski, Daniel Salz, Sebastian Goodman, Adam Grycner, Basil Mustafa, Lucas Beyer, Alexander Kolesnikov, Joan Puigcerver, Nan Ding, Keran Rong, Hassan Akbari, Gaurav Mishra, Linting Xue, Ashish Thapliyal, James Bradbury, Weicheng Kuo, Mojtaba Seyedhosseini, Chao Jia, Burcu Karagol Ayan, Carlos Riquelme, Andreas Steiner, Anelia Angelova, Xiaohua Zhai, Neil Houlsby, and Radu Soricut. Pali: A jointly-scaled multilingual language-image model, 2022. [7](#)
- [7] C. A. Christopoulos, T. Ebrahimi, and A. N. Skodras. Jpeg2000: the new still picture compression standard. In *Proceedings of the 2000 ACM Workshops on Multimedia*, page 45–49, New York, NY, USA, 2000. Association for Computing Machinery. [4](#)
- [8] A. Cohen, Ingrid Daubechies, and J.-C. Feauveau. Biorthogonal bases of compactly supported wavelets. *Communications on Pure and Applied Mathematics*, 45(5):485–560, 1992. [3](#)
- [9] Ingrid Daubechies. *Ten lectures on wavelets*. Society for Industrial and Applied Mathematics, USA, 1992. [3](#)
- [10] Jia Deng, Wei Dong, Richard Socher, Li-Jia Li, Kai Li, and Li Fei-Fei. Imagenet: A large-scale hierarchical image database. In *CVPR*, 2009. [6](#)
- [11] Prafulla Dhariwal and Alex Nichol. Diffusion models beat gans on image synthesis. In *NeurIPS*, 2021. [1](#)
- [12] Sander Dieleman. Diffusion is spectral autoregression, 2024. [2](#)
- [13] Alexey Dosovitskiy, Lucas Beyer, Alexander Kolesnikov, Dirk Weissenborn, Xiaohua Zhai, Thomas Unterthiner, Mostafa Dehghani, Matthias Minderer, Georg Heigold, Sylvain Gelly, Jakob Uszkoreit, and Neil Houlsby. An image is worth 16x16 words: Transformers for image recognition at scale. In *ICLR*, 2021. [2, 3, 4](#)
- [14] Patrick Esser, Robin Rombach, and Björn Ommer. Taming transformers for high-resolution image synthesis. In *CVPR*, 2021. [1, 2, 3, 5](#)
- [15] Patrick Esser, Sumith Kulal, Andreas Blattmann, Rahim Entezari, Jonas Müller, Harry Saini, Yam Levi, Dominik Lorenz, Axel Sauer, Frederic Boesel, Dustin Podell, Tim Dockhorn, Zion English, Kyle Lacey, Alex Goodwin, Yan-nik Marek, and Robin Rombach. Scaling rectified flow transformers for high-resolution image synthesis, 2024. [2](#)
- [16] Jiatao Gu, Shuangfei Zhai, Yizhe Zhang, Joshua M. Susskind, and Navdeep Jaitly. Matryoshka diffusion models. In *ICLR*, 2024. [3](#)
- [17] Martin Heusel, Hubert Ramsauer, Thomas Unterthiner, Bernhard Nessler, and Sepp Hochreiter. Gans trained by a two time-scale update rule converge to a local nash equilibrium. In *NeurIPS*, 2017. [1](#)
- [18] Imagen-Team-Google. Imagen 3, 2024. [2](#)
- [19] Tero Karras, Timo Aila, Samuli Laine, and Jaakko Lehtinen. Progressive growing of GANs for improved quality, stability, and variation. In *ICLR*, 2018. [3](#)
- [20] Vladimir Kulikov, Shahar Yadin, Matan Kleiner, and Tomer Michaeli. Sinddm: A single image denoising diffusion model. In *ICML*, pages 17920–17930, 2023. [3](#)
- [21] Doyup Lee, Chiheon Kim, Saehoon Kim, Minsu Cho, and Wook-Shin Han. Autoregressive image generation using residual quantization. In *CVPR*, 2022. [2](#)
- [22] Tsung-Yi Lin, Michael Maire, Serge J. Belongie, James Hays, Pietro Perona, Deva Ramanan, Piotr Dollár, and C. Lawrence Zitnick. Microsoft COCO: common objects in context. In *ECCV*. [5, 6, 7, 8, 1, 3](#)
- [23] Xiaoxiao Ma, Mohan Zhou, Tao Liang, Yalong Bai, Tiejun Zhao, Huaian Chen, and Yi Jin. Star: Scale-wise text-to-image generation via auto-regressive representations, 2024. [2](#)
- [24] Stephane Mallat. *A Wavelet Tour of Signal Processing, Third Edition: The Sparse Way*. Academic Press, Inc., USA, 3rd edition, 2008. [3](#)
- [25] Wael Mattar, Idan Levy, Nir Sharon, and Shai Dekel. Wavelets are all you need for autoregressive image generation, 2024. [3](#)
- [26] Takeru Miyato, Toshiki Kataoka, Masanori Koyama, and Yuichi Yoshida. Spectral normalization for generative adversarial networks. In *ICLR*, 2018. [5](#)
- [27] Charlie Nash, Jacob Menick, Sander Dieleman, and Peter W. Battaglia. Generating images with sparse representations. In *ICML*, 2021. [3](#)
- [28] OpenAI. Gpt-4 technical report, 2023. [1, 2](#)
- [29] Ali Razavi, Aaron van den Oord, and Oriol Vinyals. Generating diverse high-fidelity images with vq-vae-2. In *NeurIPS*, 2019. [1, 2](#)

- [30] Robin Rombach, A. Blattmann, Dominik Lorenz, Patrick Esser, and Björn Ommer. High-resolution image synthesis with latent diffusion models. In *CVPR*, 2021. 1
- [31] Tamar Rott Shaham, Tali Dekel, and Tomer Michaeli. Singan: Learning a generative model from a single natural image. In *ICCV*, 2019. 3
- [32] Dohoon Ryu and Jong Chul Ye. Pyramidal denoising diffusion probabilistic models, 2022. 3
- [33] Tim Salimans, Ian Goodfellow, Wojciech Zaremba, Vicki Cheung, Alec Radford, Xi Chen, and Xi Chen. Improved techniques for training gans. In *NeurIPS*, 2016. 1
- [34] Jascha Sohl-Dickstein, Eric Weiss, Niru Maheswaranathan, and Surya Ganguli. Deep unsupervised learning using nonequilibrium thermodynamics. In *ICML*, 2015. 1
- [35] Peize Sun, Yi Jiang, Shoufa Chen, Shilong Zhang, Bingyue Peng, Ping Luo, and Zehuan Yuan. Autoregressive model beats diffusion: Llama for scalable image generation. *arXiv preprint arXiv:2406.06525*, 2024. 2
- [36] Gemini Team. Gemini: A family of highly capable multi-modal models, 2023. 1, 2
- [37] Llama team. The llama 3 herd of models, 2024. 1, 2
- [38] Keyu Tian, Yi Jiang, Zehuan Yuan, Bingyue Peng, and Liwei Wang. Visual autoregressive modeling: Scalable image generation via next-scale prediction. In *NeurIPS*, 2024. 2
- [39] Aaron van den Oord, Nal Kalchbrenner, Lasse Espeholt, koray kavukcuoglu, Oriol Vinyals, and Alex Graves. Conditional image generation with pixelcnn decoders. In *NeurIPS*, 2016. 2
- [40] Aäron van den Oord, Nal Kalchbrenner, and Koray Kavukcuoglu. Pixel recurrent neural networks. In *ICML*, 2016. 2
- [41] Aaron van den Oord, Oriol Vinyals, and koray kavukcuoglu. Neural discrete representation learning. In *NeurIPS*, 2017. 1, 2, 3, 5
- [42] Ashish Vaswani, Noam Shazeer, Niki Parmar, Jakob Uszkoreit, Llion Jones, Aidan N Gomez, Łukasz Kaiser, and Illia Polosukhin. Attention is all you need. In *NeurIPS*, 2017. 1
- [43] Ting Yao, Yingwei Pan, Yehao Li, Chong-Wah Ngo, and Tao Mei. Wave-vit: Unifying wavelet and transformers for visual representation learning. In *ECCV*, 2022. 2
- [44] Jiahui Yu, Xin Li, Jing Yu Koh, Han Zhang, Ruoming Pang, James Qin, Alexander Ku, Yuanzhong Xu, Jason Baldridge, and Yonghui Wu. Vector-quantized image modeling with improved VQGAN. In *ICLR*, 2022. 1, 2, 3, 4, 5, 6, 7
- [45] Jiahui Yu, Yuanzhong Xu, Jing Yu Koh, Thang Luong, Gunjan Baid, Zirui Wang, Vijay Vasudevan, Alexander Ku, Yinfei Yang, Burcu Karagol Ayan, Ben Hutchinson, Wei Han, Zarana Parekh, Xin Li, Han Zhang, Jason Baldridge, and Yonghui Wu. Scaling autoregressive models for content-rich text-to-image generation. *Transactions on Machine Learning Research*, 2022. Featured Certification. 1, 3, 5, 6, 7, 8
- [46] Lijun Yu, Jose Lezama, Nitesh Bharadwaj Gundavarapu, Luca Versari, Kihyuk Sohn, David Minnen, Yong Cheng, Agrim Gupta, Xiuye Gu, Alexander G Hauptmann, Boqing Gong, Ming-Hsuan Yang, Irfan Essa, David A Ross, and Lu Jiang. Language model beats diffusion - tokenizer is key to visual generation. In *ICLR*, 2024. 2, 5
- [47] Richard Zhang, Phillip Isola, Alexei A Efros, Eli Shechtman, and Oliver Wang. The unreasonable effectiveness of deep features as a perceptual metric. In *CVPR*, 2018. 1
- [48] Zhenhai Zhu and Radu Soricut. Wavelet-based image tokenizer for vision transformers, 2024. 2

A. Ablation study

We conduct an ablation study to evaluate the effect of each of our contributions. Starting from the model denoted “SIT” in Tab. 1, we train variants reducing the number of scales, using scale-causal attention and transformer parameter-sharing independently in the encoder and decoder, using a single codebook per scale, and removing entropy loss. Tab. 5 shows the results.

B. Implementation details

B.1. Image reconstruction

For the multiscale image reconstruction experiments in Sec. 5.1, we train SIT following ViT-VQGAN [44] closely. We use the “base” encoder and “base” decoder as described in ViT-VQGAN [44]. Each transformer layer comprises a layer norm, self-attention, residual connection, followed by an MLP with layer norm, two dense layers, and a second residual connection. The “base” configuration has 12 layers, 12 heads, feature dimension of 768 that increases to 3072 in the MLP hidden layer (the hidden dimension), then back to 768. Learnable positional embedding is added to the transformer input. The codebook size is 8192 for each scale.

The tokenizer is trained for 500 000 steps with a learning rate that linearly increases up to 1×10^{-4} during the first 10% steps, then decays following a cosine schedule. We use batch size 256 and L2 weight decay with a 1×10^{-4} factor. The loss components are weighted as follows: 1.0 for L2, 0.1 for perceptual, 0.1 for adversarial, 0.25 for codebook commitment and 0.002 for codebook entropy.

B.2. Image generation

For the image generation experiments in Sec. 5.3, we train SIT models with a “small” encoder and “large” decoder as defined in ViT-VQGAN [44] and used by Parti [45]. The “small” transformer has 8 layers with 8 heads, feature dimension 512 and hidden dimension 2048. The “large” transformer has 32 layers with 16 heads, feature dimension 1280 and hidden dimension 5120. Differently from Parti, we train this tokenizer once from scratch instead of in two stages; Parti first trains a “small” encoder and decoder, then freezes the “small” encoder and trains “large” decoder.

For the generative AR-SIT, we follow the smallest architecture presented in Parti [45], with 12 layers in the text encoder and 12 decoder layers, 16 heads, 1024 feature dimensions and 4096 hidden dimensions. The text conditioning is through cross-attention.

AR-SIT is trained for 500 000 steps with a learning rate that linearly increases up to 4.5×10^{-4} during the first 10% steps, then decays exponentially. We use batch size 256 and the loss is the just the softmax cross-entropy.

B.3. Metrics

Throughout our experiments we report the following metrics:

- FID - Fréchet Inception Distance [17] estimates the distance between the distribution of generated and ground truth features obtained from a pre-trained inception model, by assuming such distributions are Gaussians and applying the Fréchet distance.
- IS - Inception Score (IS) [33] measures the entropy of a pre-trained classifier on the generated images, where low entropy is expected for good quality images.
- LPIPS - Learned Perceptual Image Patch Similarity [47] measures the distance between visual features reconstructed and ground truth images, where the features come from a pre-trained model.
- PSNR - Peak Signal-to-Noise Ratio is a pixel-wise similarity metric, the negative log of the mean-squared error.

FID and IS evaluate the quality of generated images without a corresponding ground truth, while LPIPS and PSNR are used when we have a ground truth, for example when evaluating the tokenizer.

C. Additional results

C.1. Multiscale reconstruction

Fig. 6 shows reconstruction samples at multiple resolutions, for the experiments described in Sec. 5.1.

C.2. Text-guided upsampling

In this section, we show additional results to the text-guided image upsampling experiments from Sec. 5.4. We evaluate the same task on the more challenging case where we up-sample a 16×16 input to 256×256 . Tab. 4 shows the metrics and Fig. 7 shows some examples.

Table 4. Image upsampling metrics on MS-COCO [22].

Input Resolution	FID	IS	PSNR
32×32	6.19	32.46	19.05
16×16	7.53	31.75	16.74

C.3. Additional editing results

Fig. 8 shows additional results for the text-guided image editing experiment described in Sec. 5.5.

Table 5. Ablation study. The first row corresponds to ‘‘SIT’’ in Tab. 1. Multi-codebook refers to the default of using a different codebook per scale as described in Sec. 4.1/Quantizer. Multi-transformer refers to having different transformer parameters per scale as described in Sec. 4.1/Transformers. We compare the effects of scale-causal attention independently on the encoder and decoder – while it generally reduces reconstruction accuracy, it enables the multiscale properties demonstrated in the text.

Model size	Num scales	Multi-codebook	Entropy loss	Multi-transformer Enc	Multi-transformer Dec	Scale-causal Enc	Scale-causal Dec	LPIPS	PSNR	FID	IS
Base/Base	5	✓	✓	✓	✓	X	X	0.138	25.24	1.32	197.8
Base/Base	4	✓	✓	✓	✓	X	X	0.147	24.83	1.38	193.3
Small/Large	4	✓	✓	✓	✓	X	X	0.140	25.04	1.22	203.4
Base/Base	4	✓	X	✓	✓	X	X	0.174	23.12	2.30	179.6
Base/Base	4	✓	✓	✓	✓	✓	X	0.147	24.91	1.39	191.9
Base/Base	4	✓	✓	✓	✓	X	✓	0.157	24.24	1.48	189.2
Base/Base	4	✓	✓	✓	✓	✓	✓	0.163	24.25	1.55	187.4
Base/Base	4	X	✓	✓	✓	✓	✓	0.168	24.04	1.65	185.2
Base/Base	4	✓	✓	X	✓	✓	✓	0.166	24.22	1.58	186.3
Base/Base	4	✓	✓	✓	X	✓	✓	0.167	24.12	1.71	182.5
Base/Base	4	✓	✓	X	X	✓	✓	0.168	24.10	1.70	182.5

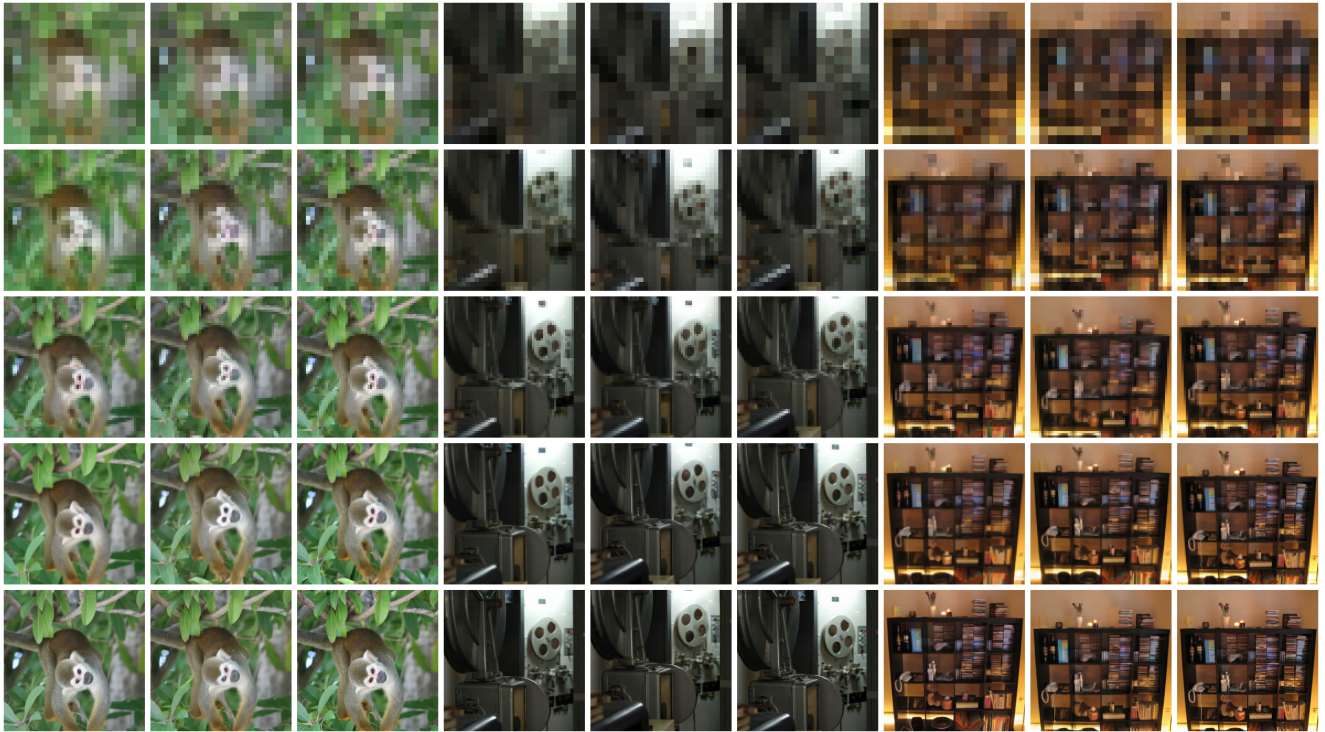


Figure 6. Multiscale reconstruction on ImageNet. Each triplet shows reconstruction from the ViT-VQGAN baseline [44], our SIT-SC-5 (Spectral Image Tokenizer with Scale-Causal attention and 5 scales), and the ground truth. Each row shows $4\times$ as many pixel inputs as the previous, with the first row corresponding to 16×16 resolution, and the last to 256×256 . Our method is naturally multiresolution, significantly outperforming the baseline on lower resolutions even when trained only on 256×256 inputs, while achieving similar accuracy on higher resolutions.

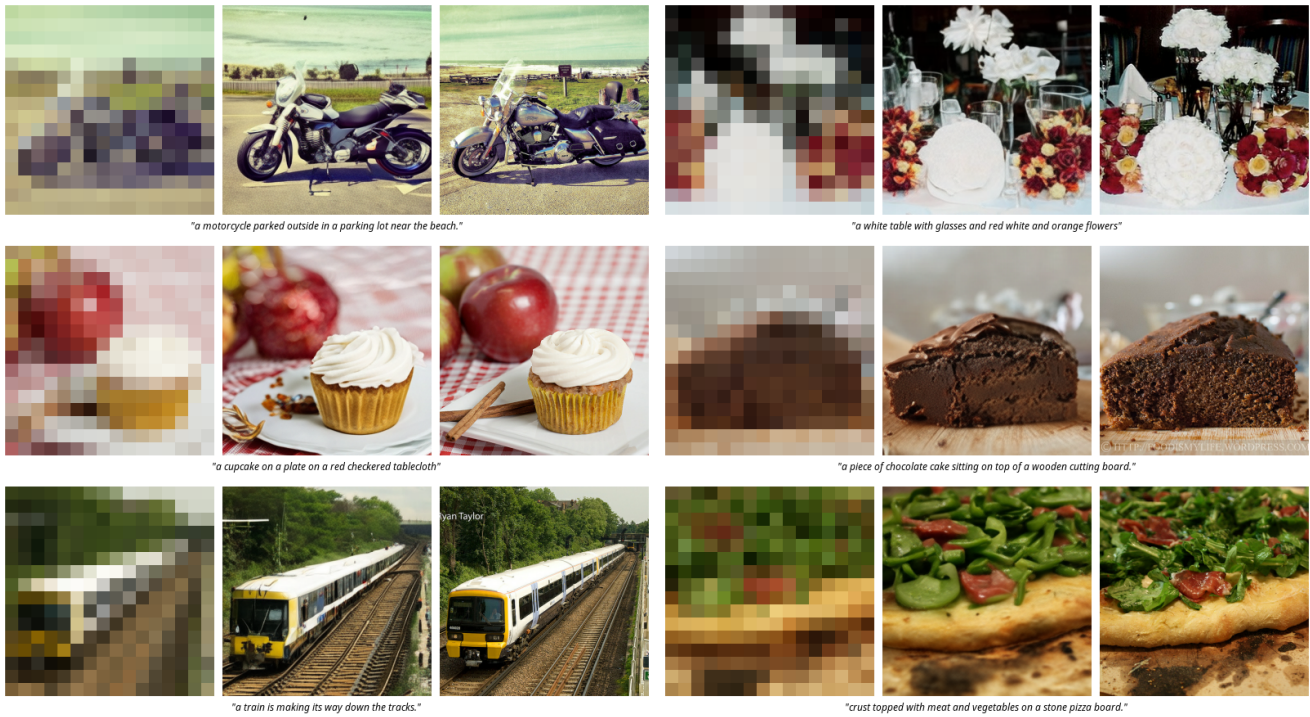


Figure 7. Additional text-guided image upsampling results. Here we consider the more challenging task of upsampling from 16×16 to 256×256 . Each triplet shows the given 16×16 image, our 256×256 reconstruction and the ground truth.

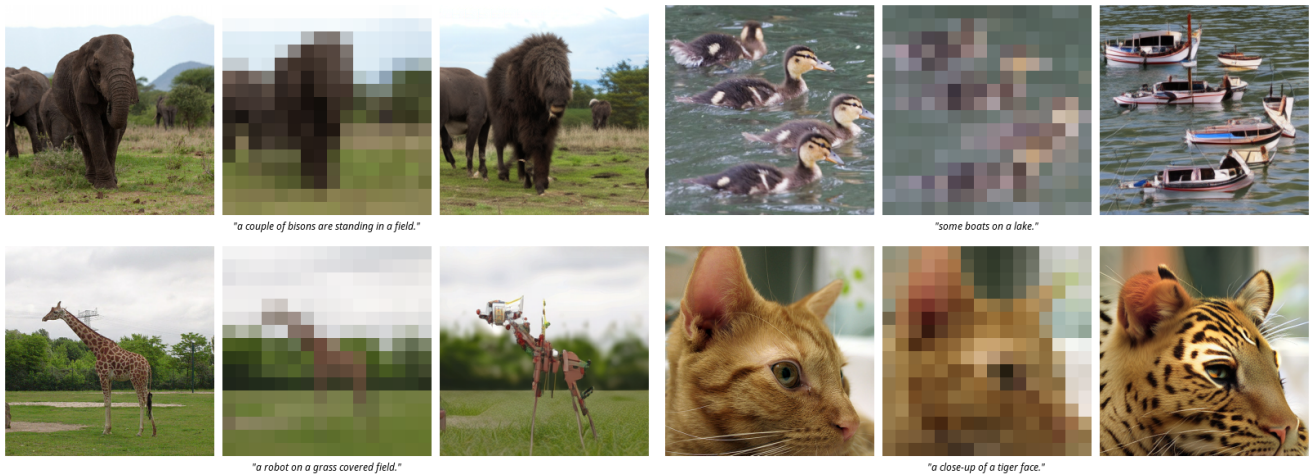


Figure 8. Additional results for text-guided image editing on MS-COCO [22]. Each triplet shows the given image, its reconstruction given only the coefficients used to start the generation, and the edited image after generating the whole sequence. The guiding prompt is shown under each triplet.